Plasmonics (2011) 6:767–772
DOI 10.1007/s11468-011-9262-z

Plasmonic Enhancement During Femtosecond Laser Drilling of Sub-wavelength Holes in Metals

Ergun Simsek · Selcuk Akturk

Received: 2 May 2011 / Accepted: 28 July 2011 / Published online: 17 August 2011

Abstract Precise ablation of metals using tightly focused femtosecond laser pulses with intensities close to the damage threshold can yield sub-wavelength, nanometer-sized holes or craters. These structures in metals can exhibit plasmonic effects, thereby affecting the interactions involved. We numerically simulate light propagation inside such holes and model the ablation process. We show that surface plasmon resonances can be excited at near-infrared and visible wavelengths. At resonance wavelengths, significant enhancement of aspect ratio is possible. Our results show that plasmonic effects are essential for the understanding of precision laser processing of metals, and they can be exploited to significantly enhance the performance of laser micro- and nano-machining.

Keywords Laser ablation · Micro- and nano-cavities · Surface plasmons · Plasmonic enhancement

Introduction

Material processing with femtosecond laser pulses yields structures with extraordinary precision due to the minimization of thermal and shock effects [1]. In this pulse duration regime, the ablation threshold is well determined and due to the involvement of nonlinear optical effects, structures even smaller than the wavelength of the laser can be generated [2–4]. This is achieved by exploiting the Gaussian transverse intensity profiles and having only the center portion of the beam exceed the ablation threshold. This method allows very high precision, only limited by shot-to-shot stability of the laser pulses. Nanometer-sized structures, such as holes or grooves, have been demonstrated in dielectrics, semiconductors, and metals. Remarkably, in transparent materials the depth of the ablated holes can even exceed the diffraction length of the focused beams, which is explained by micro-scale filament formation [5]. On the other hand, generation of high aspect ratio (depth/width) nanometer-sized holes in metals is hindered by strong absorption, and experimental results typically yield small aspect ratios [2].

Propagation of light in holes surrounded by metals can exhibit unusual properties due to excitations of surface plasmons [6]. In particular, resonant excitation and enhanced transmission of light can occur [7]. As a result, in order to understand the nanohole formation in metals through femtosecond laser ablation, plasmonic effects have to be taken into account. In this theoretical work, we show that, when holes in metals are gradually formed by consecutive laser shots, they essentially act as waveguides. The depth of the hole is determined by attenuation in this waveguide. Remarkably, as opposed to metallic waveguides with large (compared with wavelength) radii [8], the attenuation does not monotonically increase with decreasing hole diameter. Instead, due to plasmonic effects, strong reduction in attenuation, hence significant enhancement of hole aspect ratio can be achieved with proper choice of experimental parameters. These resonant effects are

E. Simsek (✉)
Department of Electrical and Electronics Engineering, Bahcesehir University, Besiktas, 34349 Istanbul, Turkey
e-mail: ergunsimsek@gmail.com

S. Akturk
Department of Physics, Istanbul Technical University, Maslak, 34469 Istanbul, Turkey

achievable at practical wavelengths of near-infrared and visible femtosecond lasers. Our results show that plasmonic effects can be critical for the understanding of laser micro- and nano-machining, and exploitation of these effects can help increase the performance of the process significantly.

In order to model femtosecond laser nano-drilling of metals, we use Gaussian beams focused to near diffraction limit. Since we are interested in behavior close to the ablation threshold [3], we take the light electric field amplitudes as multiples of the threshold value. As explained below, the amplitude of the first pulse incident on the surface determines the initial hole radius. We assume that each pulse removes a thickness determined by the skin depth. Consecutive pulses are then guided and attenuated as they propagate inside the tapered hole. The ablation process is terminated when the light amplitude inside the hole falls below the threshold.

Numerical Model

We start our analysis by considering a cylindrical hole along the z-axis, with a constant radius of R. The hole is filled with a dielectric material and the surrounding is a dispersive medium with a complex permittivity. Dielectric material is defined by its relative permittivity (ϵ_1) and relative permeability (μ_1), whereas ϵ_2 and μ_2 denote the relative permittivity and permeability of the dispersive medium, respectively. The propagating modes of such a structure can be evaluated numerically by solving a transcendental equation [9],

$$A_1 A_2 - A_3^2 = 0 \tag{1}$$

where

$$A_1 = \frac{\epsilon_1}{k_{t,1}} \frac{J_m'(k_{t,1}R)}{J_m(k_{t,1}R)} - \frac{\epsilon_2}{k_{t,2}} \frac{H_m'(k_{t,2}R)}{H_m(k_{t,2}R)},$$

$$A_2 = \frac{\mu_1}{k_{t,1}} \frac{J_m'(k_{t,1}R)}{J_m(k_{t,1}R)} - \frac{\mu_2}{k_{t,2}} \frac{H_m'(k_{t,2}R)}{H_m(k_{t,2}R)},$$

$$A_3 = \left[\frac{mk_z}{k_0 R} \left(\frac{1}{k_{t,1}^2} - \frac{1}{k_{t,2}^2} \right) \right],$$

where $k_{t,1}$ and $k_{t,2}$ are the propagation constants for the dielectric core and metallic cladding regions in the radial direction, respectively; k_z is the longitudinal component of the propagation constant; k_0 is the wavenumber in free space; $J_m(\cdot)$ and $H_m(\cdot)$ represent m^{th}-order Bessel and Hankel functions of the first kind, respectively, and prime denotes differentiation with respect to their argument. Note that the transverse components of propagation constants can be found by $k_{t,i} = \sqrt{k_0^2 \epsilon_i \mu_i - k_z^2}$ for $i = 1, 2$ and imaginary part of the $k_{t,i}$ always should be positive for the numerical solution of Eq. 1.

We assume the dielectric core to be air and for the surrounding medium, we consider three different metals: copper, silver, or gold. We use the laser wavelength of $\lambda = 800$ nm, which results in $\epsilon_2^{\text{Cu}} = -24.37 + i2.39$, $\epsilon_2^{\text{Ag}} = -25.21 + i1.74$, and $\epsilon_2^{\text{Au}} = -20.28 + i2.07$ according to experimental values for the optical constants of these metals [10]. All the materials are non-magnetic, i.e., $\mu_{\text{all}} = 1$. We solved Eq. 1 numerically for $m = 1$ and $20\,\text{nm} \leq R \leq 1\,\mu\text{m}$. Fig. 1a, b show the phase and attenuation constants as a function of core radius R for the HE_{11} mode, respectively. Note that higher-order modes ($m > 1$) are more lossy and the incoming beam profile also couples much less efficiently to them. For example, the attenuation constant for $m = 2$ mode differs roughly by one order of magnitude for the regime we consider here. Therefore, we can safely focus our consideration on the effect of the principle mode $m = 1$.

Figure 1c depicts the imaginary parts of the transverse propagation constants in metals, which are very useful to estimate the skin depth, δ. One might use analytical equations or full wave solvers to calculate δ in a dispersive material for a given wavelength. For example, in Fig. 1d, the decay of power, $P = \text{Re}\{\mathbf{E} \times \mathbf{H}^*/2\}$, is plotted for a Gaussian beam incident on a bulk copper as a function of distance from the air-copper interface, which is located at $z = 0$ and the upper half space ($z > 0$) is assumed to be copper. It is clear that power in the copper decreases with $e^{-13.2k_0 z}$, which means that $\alpha_{\text{bulk}}^{\text{Cu}} = 13.2k_0/2 = 6.6k_0$. In fact, this result agrees with the result depicted as blue solid line in Fig. 1c, where the imaginary part of the transverse propagation constant saturates to $6.6k_0$. In other words, when we calculate the dispersion diagram for a given circular hole, we also obtain δ, that is used to profile laser-drilled holes below. Note that from the same figure, we can conclude that $\alpha_{\text{bulk}}^{\text{Ag}} = 5.121k_0$ and $\alpha_{\text{bulk}}^{\text{Au}} = 4.617k_0$.

For the Gaussian transverse electric field amplitude profile, we use $E(\rho) = E_0 e^{-\rho^2/D^2}$, where E_0 is the maximum amplitude, ρ is the distance from the beam axis and D is the beam radius, which is fixed to $D = 2\lambda$ throughout this study. E_{th} denotes the minimum amplitude (ablation threshold) required to remove material from the metal surface.

Next, we consider the effect of multiple laser pulses. For femtosecond lasers with kHz repetition rates, time between pulses is sufficiently large that we can assume

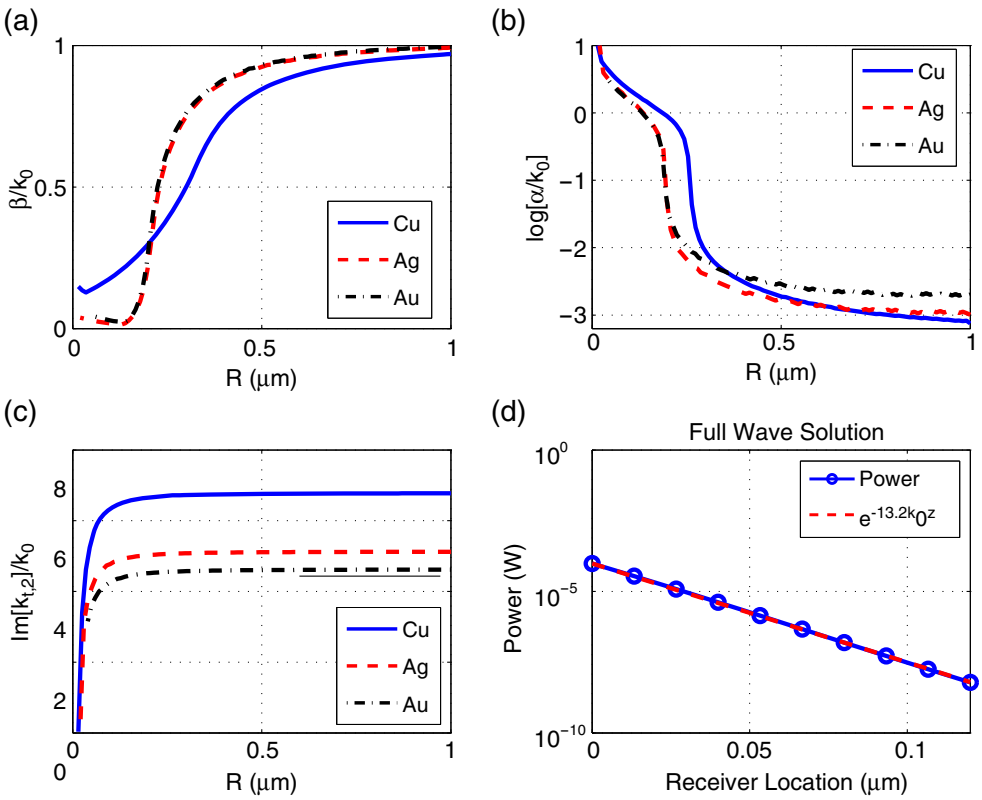

Fig. 1 Propagation constant as a function of core radius R for the HE_{11} mode. Wavelength $\lambda = 800$ nm; infinite cladding made of (*blue*) copper , (*red*) silver, and (*black*) gold; dielectric core is air. **a** Phase constant, **b** attenuation constant, **c** imaginary part of the transverse propagation constant in metal; **d** attenuation of power in bulk Cu, obtained with a commercial full-wave solver [11]

each pulse is incident on the metal at the same temperature, hence same physical properties. When the first pulse comes to the surface, it removes a disk-like layer of radius determined by the E_0/E_{th} ratio, and thickness determined by δ. When the next pulse comes, it first propagates through the hole generated by the previous, and at the end causes its own ablation. It should be noted that the laser loses its power due to ohmic losses as it propagates through the hole. Less power means smaller active ablation region which leads into a higher attenuation constant (see Fig. 1b) for subsequent pulses. Hence, the hole radius is tapered down and after some distance along the z direction, the amplitude of the light becomes smaller than the threshold value and the drilling stops. Once this crater-like structure is formed, hole profile remains unaffected by the forthcoming pulses. This physical process can be modeled easily with an iterative algorithm. At the initial step, radius of the ablated region can be found from $\rho_0 = D|\ln E_0/E_{\text{th}}|^{0.5}$. Then we can calculate the corresponding attenuation constant via a simple interpolation scheme from the solution of Eq. 1, depicted in Fig. 1b. If we chose a Δz value, that is small enough, then we can assume that the power of the laser decreases with $e^{-\alpha\Delta z}$. So in the first iteration, we obtain the new radius from $\rho_1 = D|\ln E_1/E_{\text{th}}|^{0.5}$, where $E_1 = E_0 e^{-\alpha\Delta z}$. A more general expression for the ith iteration is $\rho_i = D|\ln E_i/E_{\text{th}}|^{0.5}$, where $E_i = E_{i-1}e^{-\alpha_{i-1}\Delta z_{i-1}}$. In the consecutive steps, we update the power, attenuation, and radius and we continue until the laser amplitude, E_i, becomes smaller than the threshold. For the selection of Δz value, one can basically choose $\Delta z = \delta$. However, for smoother results and especially for the case where E_0 is close to E_{th}, we should choose smaller Δz, for example $\Delta z = \delta/100$. Another advantage of using small Δz is its efficacy to represent a tapered waveguide's behavior by averaging the behaviors of infinitely long cylinders as explained at the end of the "Numerical Results" section.

Numerical Results

By applying the method explained above to bulk silver, copper and gold, we generate the hole profiles for different E_0/E_{th} ratios at laser wavelength of 800 nm. In Fig. 2, we plot three dimensional shape of the holes drilled into silver for $E_0 = 1.02E_{\text{th}}$ and $E_0 = 1.05E_{\text{th}}$, where $\rho_0 = 230.6$ and $d = 51.5$ nm for the former case and $\rho_0 = 353.4$ and $d = 932.9$ nm for the latter case (d denotes the depth of the cavity). If we use gold, d values become 38.4 and 586 nm for the same E_0/E_{th} ratios, respectively. If the material is copper, then d values become 38.1 and 652.1 nm, respectively. Note

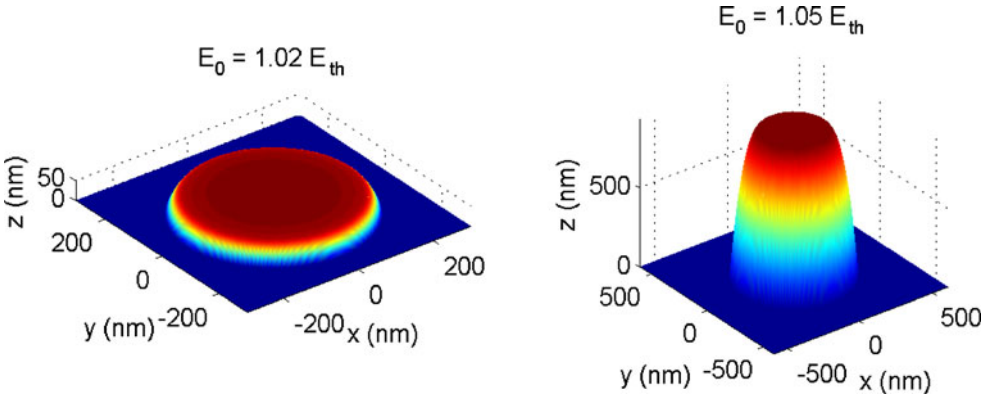

Fig. 2 Numerically obtained hole profiles in *silver*: **a** $E_0 = 1.02E_{\text{th}}$, **b** $E_0 = 1.05E_{\text{th}}$ for $\lambda = 800$ nm, $\epsilon_2^{\text{Ag}} = -25.21 + i1.74$

that since we fixed the E_0/E_{th} ratio, ρ_0's are same for all metals.

In order to understand the effect of the laser wavelength and plasmonic resonances, we analyze the crater depth-wavelength dependency. We use gold as the host material and we choose the initial laser power according to $E_0 = E_{\text{th}}/e^{-\rho_0^2/D^2}$, for a fixed E_{th} value and set of desired ρ_0 values. Since we are interested in sub-wavelength holes, we chose ρ_0 values between 0.15 and 0.4 μm and applied the numerical method explained above for $400 < \lambda < 1{,}100$ nm. Similar to the extinction cross sections of metal nanoparticles, the crater depth has maxima around the metal's plasmon frequency and we refer to this as resonance depth, d_{res}.

Figure 3a shows crater depth-wavelength dependency for different ρ_0 values. Each case is normalized with the maximum depth occurring at the plasmonic resonance, d_{res}. Clearly, cavity depth changes dramatically with respect to laser's wavelength. For example, for $\rho_0 = 0.4$ μm case, $d_{\lambda:800\text{ nm}} = 6.2 \times d_{\lambda:515\text{ nm}}$. In Fig. 3a, we also observe the red shift in the resonance wavelengths, as we increase the cavity opening. With the help of a simple interpolation scheme, we estimate the resonance values for wavelength and depth, and we plot them as blue and red lines in Fig. 3b. We can observe that, resonance depth increases exponentially as we increase the diameter of the initial opening. For comparison, in the same figure we also plot the maximum depth for the case of constant wavelength of 515 nm (green line). Comparison with the resonant case clearly underlines the enhancement of the hole aspect ratio when appropriate wavelength is used.

In order to investigate the plasmonic enhancement effects on the near-field profiles, we run two more simulations using [11] as follows. We assume a tapered cylindrical crater (in other words, a conical frustum with $\rho_{\text{initial}} = 300$ nm, $\rho_{\text{final}} = 240$ nm, and $d = 250$ nm) drilled inside a gold layer with a thickness of 500 nm, and we numerically calculate the total fields at two different wavelengths: (a) $\lambda = 515$ nm and (b) $\lambda =$ 800 nm. The results are shown in Fig. 4. In this figure, electric field lines are depicted with arrows (since electric field lines are towards the $\hat{x}$-axis, we see their

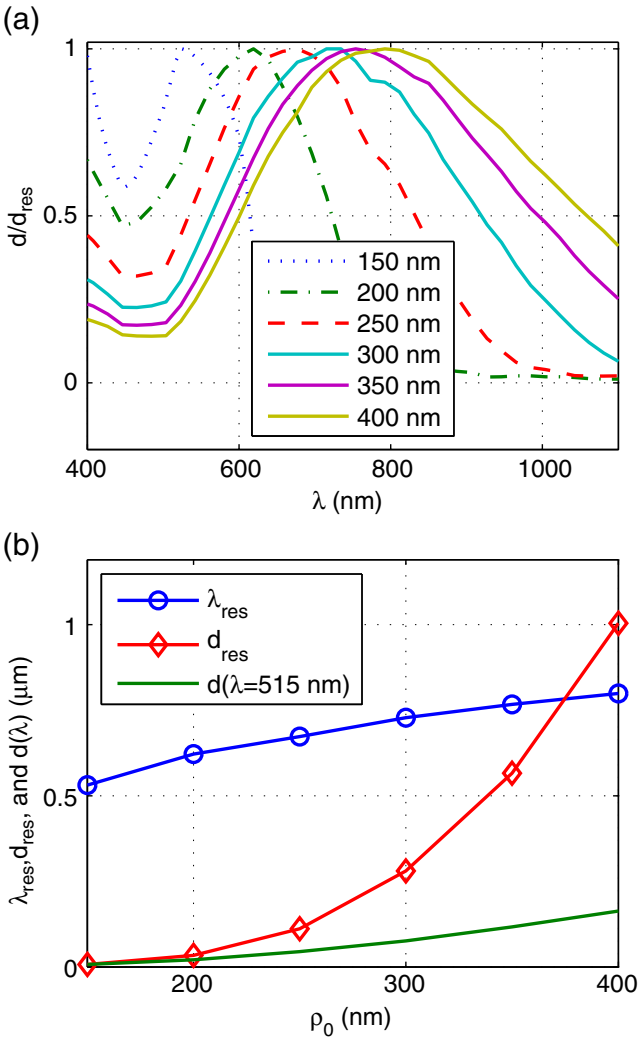

Fig. 3 **a** Cavity depth vs. wavelength for $\rho_0 = 0.15, 0.2, 0.25, 0.3, 0.35, 0.4$ μm. **b** The change in the resonance wavelength (*blue line*) and depth at that resonance (*red line*), when we change the width of the cavity opening. *Green line* depicts the maximum depth for the case of constant wavelength of 515 nm

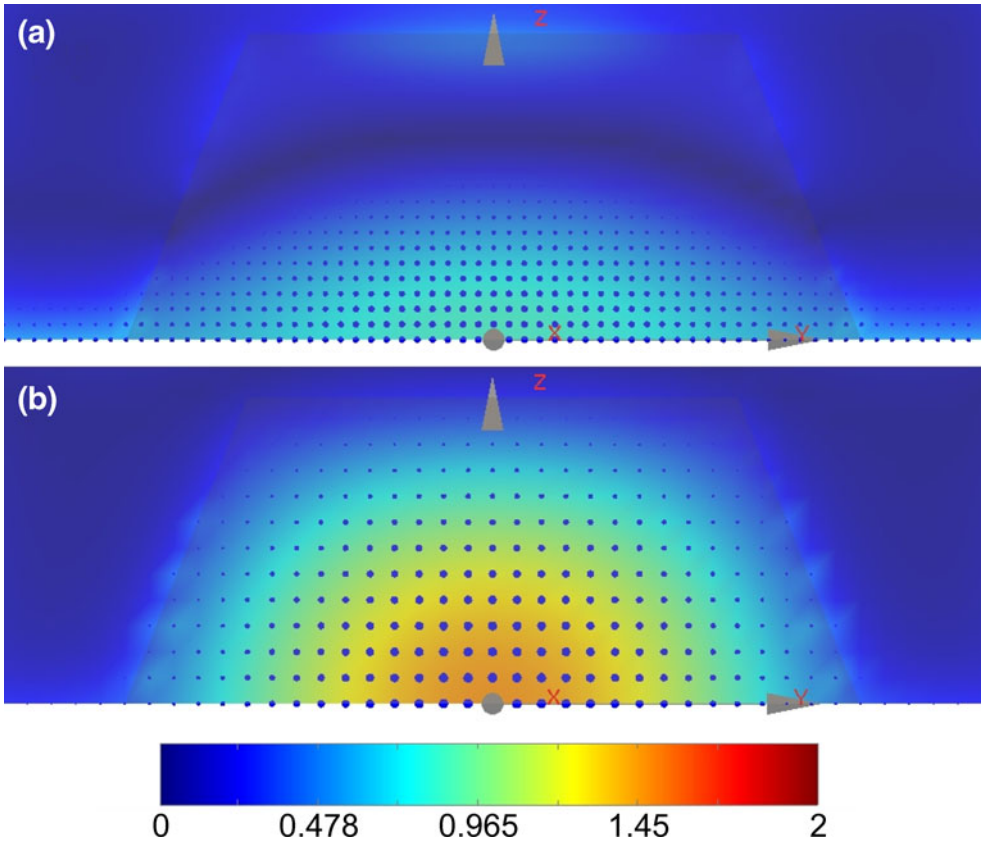

Fig. 4 Simulation results: Gaussian beam penetration to a tapered cylindrical crater (with $\rho_{\text{initial}} = 300$ nm, $\rho_{\text{final}} = 240$ nm, and $d = 250$ nm) drilled inside a gold layer **a** $\lambda = 515$ nm and **b** $\lambda = 800$ nm. In both subplots, the semi-transparent trapezoid shows the edges of the conical frustum

heads). Bigger arrow (head) means stronger electric field. The magnitude of the magnetic field multiplied by the impedance of free space, $\eta = 377\ \Omega$, is shown by color. In both simulations, the Gaussian beam width is taken to be 2λ. In the absence of plasmonic effects, we would expect to have more field confinement for the case of smaller wavelength. However, as shown in Fig. 4, we have the opposite result here: the fields with longer wavelength penetrate more. This observation agrees with the results shown with the cyan line in Fig. 3a, where our theoretical model claims that for a fixed ρ_0, the depth of the crater for $\lambda = 800$ nm is more than three times larger than the depth of the crater for $\lambda = 515$ nm.

Lastly, we would like to emphasize that using small Δz (e.g., $\Delta z = \delta/100$) allows us to approximate the loss in a tapered waveguide based on the knowledge of attenuation in infinitely long circular cylinders. Let us explain this perturbation-like approach by analyzing the field attenuation for $\rho = 300$ nm and $\lambda = 800$ nm case used in the previous example. According to our model, electric field is decreased by 1.26% at the end of 206th step, which gives $d_i \approx 200$ nm, $\rho_i \approx 240$ nm, and hence the power is decreased by 1.27 dB/μm throughout this structure. The attenuation constant values for infinitely long cylinders with radii of 300 and 240 nm are 0.99 and 1.89 dB/μm, respectively. In other words, our method yields an approximate effective attenuation constant which is between these two extreme cases. In order to evaluate the accuracy of this approach, we use the commercial full wave solver [11] assuming a hole tapered inside 200-nm thick Au layer with 300 nm of initial radius and 240 nm of final radius, and we calculate the attenuation constant as 1.22 dB/μm. The difference between attenuation constants calculated numerically and theoretically is only 4.1%, and this difference does not have any significant effect on the plasmonic enhancements we mentioned above.

Conclusions

In conclusion, we numerically analyze generation of nanometer-sized holes in metals by tightly focused femtosecond laser pulses with intensities close to the damage threshold. We show that plasmonic effects in such holes affect the ablation process. If the laser wavelength is resonant, significant enhancement of aspect ratio is possible.

Acknowledgement This work was supported by the Scientific and Technological Research Council of Turkey (TUBITAK, grant numbers 110T330 and 110E002).

References

1. Stuart BC, Feit MD, Herman S, Rubenchik AM, Shore BW, Perry MD (1996) Nanosecond-to-femtosecond laser-induced breakdown in dielectrics. Phys Rev B 53:1749
2. Pronko PP, Dutta SK, Squier J, Rudd JV, Du D, Mourou G (1995) Machining of sub-micron holes using a femtosecond laser at 800 nm. Opt Commun 114:106–110
3. Joglekar AP Liu H, Meyhöfer E, Mourou G, Hunt AJ (2004) Optics at critical intensity: applications to nanomorphing. Proc Natl Acad Sci USA 101:5856–5861
4. Englert L, Rethfeld B, Haag L, Wollenhaupt M, Sarpe-Tudoran C, Baumert T (2007) Control of ionization processes in high band gap materials via tailored femtosecond pulses. Opt Express 15:17855–17862
5. Herbstman JF, Hunt AJ (2010) High-aspect ratio nanochannel formation by single femtosecond laser pulses. Opt Express 18:16840–16848
6. Ebbesen TW, Lezec HJ, Ghaemi HF, Thio T, Wolff T (1998) Extraordinary optical transmission through sub-wavelength hole arrays. Nature 391:667–669
7. Genet C, Ebbesen TW (2007) Light in tiny holes. Nature 445:39–46
8. Marcatili EA, Schmeltzer R (1964) Hollow metallic and dielectric waveguides for long distance optical transmission and lasers. Bell Syst Tech J 43:1783–1809
9. Stratton JA (1941) Electromagntic theory. McGraw-Hill, New York
10. Rakic D, Djurisic AB, Elazar JM, Majewski ML (1998) Optical properties of metallic films for vertical-cavity optoelectronic devices. Appl Opt 37:5271–5283
11. Wavenology from Wave Computation Techonologies, Inc., Durham, NC